High-Throughput Computational Screening of Chromophores for Dye-Sensitized Solar Cells

ARTICLE *in* THE JOURNAL OF PHYSICAL CHEMISTRY C · MAY 2011

Impact Factor: 4.77 · DOI: 10.1021/jp2026847

2 AUTHORS, INCLUDING:

Natalia Martsinovich
The University of Sheffield
60 PUBLICATIONS **865** CITATIONS

SEE PROFILE

THE JOURNAL OF PHYSICAL CHEMISTRY C

ARTICLE

pubs.acs.org/JPCC

High-Throughput Computational Screening of Chromophores for Dye-Sensitized Solar Cells

Natalia Martsinovich* and Alessandro Troisi*

Department of Chemistry and Centre for Scientific Computing, University of Warwick, Coventry, West Midlands CV4 7AL, United Kingdom

Supporting Information

ABSTRACT: Electron injection from a photoexcited chromophore into semiconductor (TiO_2) nanoparticles is one of the key electron transfer processes in dye-sensitized solar cells. We describe our model for calculations of electron injection times, which is based on partitioning the semiconductor−chromophore system into fragments (TiO_2 slab with adsorbed chromophore's anchoring group, and an isolated chromophore), and calculating the imaginary part of the self-energy from the electronic properties of the fragments: density of states of TiO_2 slab, TiO_2−anchoring group coupling, and chromophore's wave function coefficients. The electronic properties of the semiconductor and its interface with the chromophore's anchoring group are reused for all chromophores with the same anchoring group (carboxylic acid in this study), and only a calculation of the isolated chromophore's lowest unoccupied molecular orbital is required for each chromophore. We use this model to calculate electron injection times for a large set of organic chromophores, including, e.g., perylene dyes and biisonicotinic acid, on TiO_2 rutile (110) and anatase (101) surfaces. The calculated injection times are in good agreement with reported experimental injection times or light conversion efficiencies of solar cells based on these dyes. Our model is computationally efficient and allows us to make reliable predictions of electron injection times for families of chromophores sharing the same adsorption chemistry.

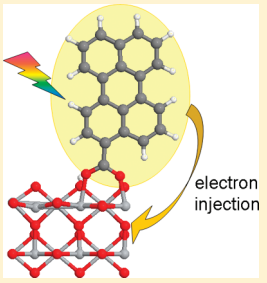

1. INTRODUCTION

Solar cells provide an opportunity to harness solar light energy by converting it to electricity.[1−4] The dye-sensitized solar cell (DSSC) is a very promising type of solar cell with efficiency of converting solar light to electricity of up to 11%.[5,6] It is based on semiconductor nanoparticles (typically, TiO_2, or, less commonly, ZnO) covered with metal−organic or organic dyes (chromophores), which act as a sensitizer. Photoexcited electrons in the dye are then transferred to the semiconductor (the electron injection process), resulting in charge separation at the dye−semiconductor interface. The electrons flow through the semiconductor to one of the electrodes; the oxidized dye is restored by a redox pair in electrolyte solution, usually the iodide/triiodide mixture; the redox pair, in turn, is regenerated at the counter-electrode. The theoretical maximum efficiency for single-junction solar cells is ca. 30%; however, the efficiency of real solar cells never approaches this due to various loss processes. In DSSCs, the main loss mechanisms are charge recombination (back transfer) at the dye−semiconductor interface, capture of electrons by the redox couple, and the decay of the dye's excited state.[7,8]

Rates of the various electron transfer processes have been measured for some dyes used in DSSCs, such as ruthenium complexes,[9,10] coumarin dyes,[11−18] perylene derivatives,[19−24] and pyridine derivatives,[25−27] using infrared and visible transient absorption spectroscopy,[9,10,13−16,18−20,24] Raman spectroscopy,[17] fluorescence up-conversion spectroscopy,[11] resonant photoemission,[24−26] and two-photon photoemission spectroscopy.[21−23] Measurements show that electron injection is typically the fastest process, which occurs on the time scale of femtoseconds to hundreds of femtoseconds for most dyes.[9−27] For comparison, the time scale for charge recombination is hundreds of picoseconds to nanoseconds.[17,28] Thus, in most DSSCs, processes other than electron injection (e.g., regeneration of the redox couple and electron transport through the semiconductor particles) are likely to be the efficiency determining steps. However, if electron injection is slow, for example, on the same time scale as recombination, the DSSC is going to have a very poor performance. Thus, we need to understand the factors that control electron injection, in order to design dyes that provide rapid electron injection and make efficient solar cells.

Several theoretical approaches have been put forward to model the rates of electron transfer at the semiconductor−dye interface. As a first approximation, electron injection time can be calculated from the partial density of states (PDOS) of the semiconductor−dye system as the inverse of the width of the adsorbate's excited states.[29−34] This approach follows the Anderson−Newns model for adsorbates on metals[35,36] and considers the broadening of the excited state as a measure of lifetime of this state, but it is very dependent on a correct identification of the shape of the PDOS and gives no information on dynamics. Nonadiabatic molecular dynamics has been used by

Received: March 22, 2011
Revised: May 4, 2011
Published: May 20, 2011

Prezhdo's group to simulate electron transfer processes on a tens-of-femtoseconds time scale, to estimate electron transfer rates and distinguish between adiabatic and nonadiabatic electron transfer pathways.[37−40] A time-dependent density-functional theory (TD-DFT) study by De Angelis et al.[41] suggested that the charge transfer mechanism may change from nonadiabatic to adiabatic as a result of proton transfer from the dye to the surface. A reduced density matrix approach has been proposed by Venkataraman et al. to model proton-coupled electron transfer at molecule−semiconductor interfaces.[42] Ab initio molecular dynamics combined with a time-dependent Hückel Hamiltonian description of electron dynamics has been used by Batista et al. to model dye-semiconductor electron transfer and subsequent charge delocalization in TiO_2 crystals.[43,44] Electron transfer dynamics and rates have also been studied by Thoss et al. using a representation of Hamiltonian in a basis of localized donor and acceptor states, with the parameters of the Hamiltonian taken from ab initio calculations,[45−47] in an approach similar to this work. A model of electron transfer by May et al.[19,48] uses a diabatic-like separation of the whole system into molecular and semiconductor states and considers the ground and first excited state for the dye together with a large number of states in the conduction band of the semiconductor; the parameters of the Hamiltonian in this phenomenological model are fitted to measured spectra, i.e., this model relies on prior experimental results.

A common feature in these models (apart from the last one) is that they require a full simulation of the semiconductor−dye system, which demands a lot of computer time and, necessarily, limits the scope of the simulations to one or few dyes. Here, we describe and use a model that partitions the semiconductor−dye system into three subsystems: (i) semiconductor slab, (ii) interface of the slab with the dye's anchoring group, and (iii) complete dye; these three subsystems are modeled separately using first principles density-functional theory (DFT) calculations. The results of simulations of systems (i) and (ii) are transferable, i.e., the electronic properties of the first two subsystems (the most time-consuming calculations) can be modeled once and reused for all dyes that have the same anchoring group. Electron injection rates are then calculated from the imaginary part of the self-energy, which is evaluated using the electronic Hamiltonian (the coupling between the semiconductor's and dye's energy states), the semiconductor's density of states, and the dye's lowest unoccupied molecular orbital (LUMO) (used as an estimate of the highest occupied molecular orbital (HOMO) of the dye in its excited state).

This partitioning, initially proposed in ref 49, was only used in ref 49 in conjunction with cluster calculations, whose accuracy is always difficult to evaluate. In this work we use a full periodic model of the semiconductor (TiO_2) surfaces, rather than a finite cluster. The periodic model gives a more reliable description of surface−adsorbate interaction, which is one of the most difficult computational chemistry problems. However, these are also very computationally demanding calculations, because the semiconductor surface area required in the periodic model increases with the size of the adsorbate, and very large surfaces may be needed to accommodate large chromophores. Therefore, partitioning of the system is particularly useful in periodic calculations, as it strongly reduces the size of the calculated surface−adsorbate system and allows us to recycle this computationally demanding part of the calculation. As a summary, our partition model means that full calculations of the semiconductor−dye system can be avoided: for any new dye, only a calculation of the isolated dye is needed, in combination with our library of results on TiO_2 density of states and the couplings at the semiconductor−anchoring group interface. We use this model to calculate electron injection rates for a large set of organic dyes on TiO_2 rutile and anatase surfaces (in the current study, dyes with carboxylic group as the anchoring group are considered).

The paper is organized as follows. The details of our theoretical model and the computational procedure are outlined in Section 2. In Section 3, we present our calculated electron injection times for a large set of organic dyes on TiO_2 rutile (110) and anatase (101) surfaces. We compare the calculated injection times with experimental values (where available) and with light conversion efficiency values for DSSC based on these dyes, and show that there is good agreement between our theoretical values and the experiments. This suggests that our method can be reliably used as a predictive tool to evaluate electron injection efficiency of candidate dyes before they are synthesized. Finally, we discuss the accuracy of our predictions of electron injection times.

2. METHODS

2.1. Theoretical Background. The charge injection process consists of charge transfer between an orbital localized on the chromophore molecule and one of the one-electron states of the continuum formed by the semiconductor's conduction band states. The general behavior of a system initially prepared in a single state $|s\rangle$, which is coupled to a manifold of states $\{|l\rangle\}$, is very well-known, as it is encountered in many problems of chemical physics.[50,51] The probability of finding the system in state $|s\rangle$ decreases exponentially with time with a rate $\Gamma_{ss}(E_s)$, dependent on the coupling V_{sl} between the initial and final states and their energies E_s and $\{E_l\}$. The expression for such rate can be derived from second-order perturbation theory, but it is more general to describe the same process using the theoretical framework of Green's functions and partitioning theory. The effect of states $\{|l\rangle\}$ on state $|s\rangle$ can be described by an extra energy term, the complex self-energy, to be added to E_s. The real part of the self-energy corresponds to a shift of the energy of E_s due to the presence of the manifold of states $\{|l\rangle\}$; the imaginary part $\hbar\Gamma_{ss}$, always positive, can be seen as an energy broadening of $|s\rangle$, also due to the manifold. This broadening, divided by $\hbar$, corresponds to the inverse lifetime of state $|s\rangle$ or, equivalently, to the rate of transfer from state $|s\rangle$ to one of the states $\{|l\rangle\}$. $\Gamma_{ss}(E)$ is defined as a function of the energy:[50,51]

$$\hbar\Gamma_{ss}(E) = 2\pi \sum_l V_{sl} V_{sl}^* \delta(E - E_l) \qquad (1)$$

where $\delta(E)$ is the Dirac delta function. $\Gamma_{ss}(E)$ is to be evaluated at the injection energy $E = E_s$ to obtain the injection rate.

For the charge injection in a DSSC, the states $|s\rangle$ and $|l\rangle$ are associated with the donating molecular orbital on the adsorbed molecule and the conduction band orbitals in the semiconductor. To calculate $\Gamma_{ss}(E)$ for a realistic system, they can be expressed in a localized basis set, for example, as a linear combination of atomic orbitals: $|s\rangle = \Sigma_m c_m \chi_m$ and $|l\rangle = \Sigma_k C_{kl} \phi_k$. Here, $\{\phi_k\}$ is the basis set for the semiconductor, $\{\chi_m\}$ is the basis set for the molecule, and indices k (or k') and m (or n) refer to the semiconductor's and the molecule's basis functions, respectively. Then, the coupling V_{sl} between the states $|s\rangle$ and $|l\rangle$ can be expressed via the coupling between localized basis functions of

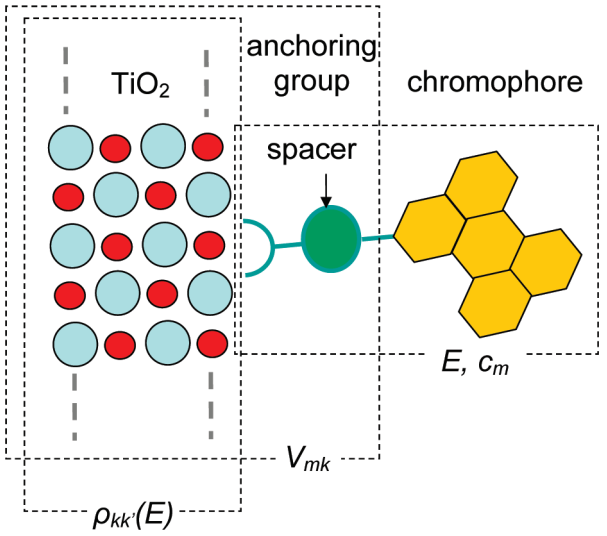

Figure 1. Schematic showing a TiO_2 surface with an adsorbed molecule. The anchoring group (including an optional spacer) and the chromophore part of the molecule are highlighted. The dotted rectangles indicate the three partitions of the system (surface only, surface with small adsorbate, and chromophore with spacer) used in this paper. Each partitioning is used to compute one or two terms ($\rho_{kk'}(E)$, V_{mk}, c_m, E) entering the definition of the injection rate (defined in the manuscript), as indicated in the figure.

the molecule and localized basis functions of the semiconductor, $\{V_{mk}\}$, so that expression 1 for $\Gamma_{ss}(E)$ becomes

$$\hbar\Gamma_{ss}(E) = \sum_{m,n} \Gamma_{mn}(E) c_m c_n^* \tag{2}$$

$$\hbar\Gamma_{mn}(E) = 2\pi \sum_l \sum_{k,k'} V_{mk} V_{nk'}^* C_{lk} C_{lk'}^* \delta(E - E_l) \tag{3}$$

In eq 3, we can separate the terms that describe the semiconductor surface alone (basis set coefficients C_{lk}) and the terms that describe the interface between the slab and the molecule (couplings V_{mk}). The former terms can be grouped together as the energy-dependent local density of states:

$$\rho_{kk'}(E) = \sum_l C_{lk} C_{lk'}^* \delta(E - E_l) \tag{4}$$

Then, eq 3 becomes[49]

$$\Gamma_{mn}(E) = \frac{2\pi}{\hbar} \sum_{k,k'} V_{mk} V_{nk'}^* \rho_{kk'}(E) \tag{5}$$

Finally, if the basis set is nonorthogonal, eq 5 should be modified as follows:[52]

$$\Gamma_{mn}(E) = \frac{2\pi}{\hbar} \sum_{k,k'} (ES_{mk} - V_{mk})(ES_{nk'} - V_{nk'})^* \rho_{kk'}(E) \tag{6}$$

In practice, the following steps are required to evaluate electron injection time using the above equations: (i) computation of the local density of states of the semiconductor $\rho_{kk'}(E)$, (ii) computation of the coupling $\{V_{mk}\}$ between the semiconductor's and molecule's localized basis functions, and (iii) computation of the molecule's basis set coefficients $\{c_m\}$ and the energy of the molecule's LUMO, which is the injection energy E in eq 5. Figure 1 illustrates the partitioning of the TiO_2—chromophore system and the properties ($\rho_{kk'}(E)$, $\{V_{mk}\}$, $\{c_m\}$, E) derived from each of the system's parts.

2.2. Partitioning of the System and the Choice of Molecules. Equations 2—6 contain terms that describe the properties of the semiconductor surface ($\rho_{kk'}(E)$), the semiconductor—chromophore interface (V_{mk}), and the chromophore itself (c_m, $E = E_s$). It is intuitively obvious (and can be demonstrated by inspecting the **V** matrix) that the coupling terms V_{mk} between the semiconductor's and molecule's localized basis functions are significantly different from zero only for those m, k that are at or near the semiconductor—dye interface. Hence, it is sufficient to use $\rho_{kk'}(E)$ matrix elements only for k, k' close to the semiconductor surface. Therefore, we can represent a semiconductor surface with a slab, which is periodically repeated in two dimensions and has a finite depth—a widely used approach for modeling surfaces. Theoretical studies of adsorbates on TiO_2 typically use two to four-layer slabs.[29,30,33,53,54] In our recent study of TiO_2 slabs,[55] we showed that relatively small 2- or 3-layer anatase slabs are sufficiently large to model the anatase (101) surface, although thicker slabs are needed to accurately describe the rutile (110) surface.

To obtain V_{mk} values, we can do a calculation of a dye adsorbed on a slab. However, these calculations are extremely time-consuming, and we cannot hope to use this method to screen a large number of potential chromophores. As we can expect V_{mk} values to be large only in the interface region, we can, for the purpose of calculating V_{mk} matrix elements, consider the interface of the semiconductor slab with the chromophore's anchoring group and omit the rest of the chromophore (exploiting the fact that V_{mk} values for m not belonging to the anchoring group are vanishingly small).

Attachment chemistry, i.e., the mode of adsorption of the dye to the semiconductor surface, is one of the most complicated aspects of the semiconductor—chromophore system. There may be several alternative adsorption modes, e.g., molecular, bridging, or chelating.[53,56,57] Fortunately, there are few types of anchoring groups that are found in common DSSC chromophores: hydroxyl, carboxylic, and phosphonic acid. In this work, we consider chromophores that attach to the surface via a carboxylic group, and use benzoic acid to model these chromophores' anchoring group. Earlier DFT studies showed that carboxylic acids (e.g., formic, acetic, and benzoic acid) adsorb on the TiO_2 rutile (110) surface in the dissociative bridging bidentate configuration;[56] both dissociative bidentate and molecular (nondissociative) adsorption is possible for carboxylic acids on anatase (101), the latter being slightly more energetically favorable.[53] Computational studies showed that these few adsorption modes are stable for several different small carboxylic acids (e.g., formic, acetic, or benzoic acid behave in the same way),[53,55,58] and we can expect that, similarly, these will be the adsorption modes adopted by large carboxylic acid chromophores on TiO_2.

2.3. Computational Details. DFT calculations performed using SIESTA[59] were used to obtain the input data for eqs 2—6: the energies of Kohn—Sham states E_l and E_s, basis set coefficients C_{lk} and c_m, matrix elements V_{mk} and S_{mk}. The coupling terms V_{mk} in eqs 5 and 6 are the (m,k) elements of the Kohn—Sham Hamiltonian matrix **H**. Equations 2—6 are derived for a system with a single adsorbed dye, i.e., a nonperiodic system, while the efficient evaluation of the dye—adsorbate interaction in this work is performed via periodic calculations. For periodic systems, such as TiO_2 slab in this work, several **k**-points are used for accurate sampling of the Brillouin zone, and there are as many

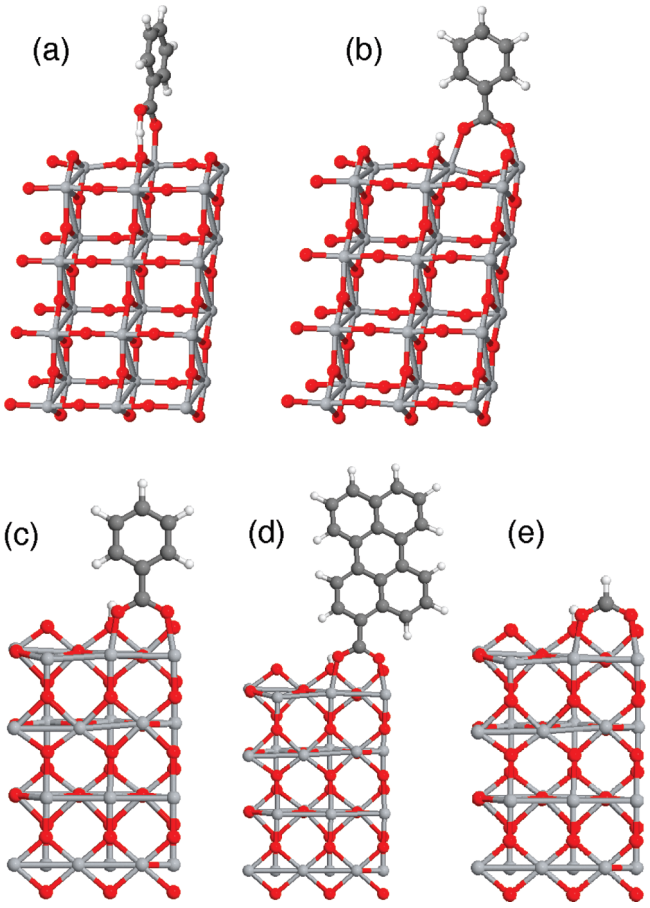

Figure 2. Benzoic acid adsorbed on (a,b) a four-layer anatase (101) slab in the (a) nondissociative and (b) dissociative configurations, and (c) on a four-layer rutile (110) slab in the dissociative configuration. (d) Full chromophore (labeled **h** in Figure 3) and (e) formic acid adsorbed on a four-layer rutile (110) slab in the dissociative configuration.

H matrices as the number of **k**-points used. Considering that H_{mk} values decrease exponentially with the distance between m and k basis orbitals, and that atomic orbitals involved in the chemisorption are far from their images, $H^{\mathbf{k}}_{mk}$ is very weakly dependent on **k**. We used the **H** matrix calculated at the Gamma (Γ) point—the point that corresponds to the minimum of the rutile and anatase conduction band. We believe that (1×3) slabs used here are sufficiently large, and the Γ-point **H** matrix is sufficient for accurate representation of these TiO_2 slabs' electronic structure. Similarly, the S_{mk} terms in eq 6 are the elements of the overlap matrix **S**.

We used benzoic acid as an anchoring group and modeled its adsorption on rutile (110) and anatase (101) slabs of various thicknesses (two to four-layer anatase (101) slabs and two to five-layer rutile (110) slabs were used; a layer is defined as in ref 55). We considered nondissociated (molecular) and dissociative adsorption configurations on anatase (101), shown in Figure 2a,b, and dissociative adsorption on rutile (110), Figure 2c. We used generalized gradient approximation (GGA) with the Perdew–Burke–Ernzerhof (PBE) functional[60] for exchange and correlation, Troullier-Martins norm-conserving pseudopotentials, with the semicore states for Ti treated explicitly, and a double-ζ polarized (DZP) basis set for all atoms, except Ti for semicore states, for which a minimal basis set was used. Note that the localized basis set in SIESTA is normalized but nonorthogonal, and thus eq 6 should be used, rather than eq 5. The details of these calculations were the same as those described in our methodological paper,[55] where we investigated the performance of different DFT approximations and implementations in the studies of molecular adsorbates on TiO_2.

In the same paper[55] we showed that the GGA PBE treatment of TiO_2 slabs gives a description of the electronic structure that is qualitatively similar to the more accurate B3LYP hybrid functional treatment: while the band gap is underestimated, the shape of the density of states and the contributions of surface and bulk-like TiO_2 layers to the total DOS are very similar in PBE and B3LYP. Thus, PBE results for the electronic properties of TiO_2 slabs and TiO_2-adsorbate interfaces can be used, rather than the more accurate but more time-consuming B3LYP calculations. Moreover, despite the approximations used in SIESTA, its description of the electronic structure of TiO_2 and TiO_2-adsorbate systems was very similar to that given by the more accurate plane wave pseudopotential calculations (using QUANTUM ESPRESSO) or all-electron calculations (using CRYSTAL06).

The periodic-boundary description of TiO_2 slabs used in this work is more accurate than the finite cluster embedded in point charges;[49] the latter technique is known to induce a nonphysical polarization of anions,[61] making the results very dependent on an appropriate choice of the embedding technique;[62] clusters' band gaps tend to be larger than those of TiO_2 bulk or slabs and vary with cluster size;[31] a recent TD-DFT study of alizarine on TiO_2[63] also showed that the position of the adsorbate's LUMO below or inside the "conduction band" of the cluster varies depending on the cluster size. We showed in ref 55 that adsorption of carboxylic acids somewhat affects the local density of states of the surface atoms, especially near the band edges. Therefore, we used the surface–anchoring group system, rather than the bare surface used in ref 49 to obtain the coefficients C_{lk} used to calculate $\rho_{kk'}(E)$. The local density of states $\rho_{kk'}(E)$ was evaluated as a sum over all states l in the valence and conduction band of the slab. The same TiO_2–adsorbate systems were used to obtain the couplings between the slab and molecule's basis functions, V_{mk}.

We expect that the density of states of TiO_2 slabs is very similar in TiO_2–anchoring group and TiO_2–complete dye systems. Indeed, we have checked that the densities of states and band structures of TiO_2–anchoring group and TiO_2–dye systems for few selected dyes (considered in Section 3.3) are very similar (apart from the positions of the adsorbates' states), and there is no gap inversion—the band gap of rutile remains direct, and anatase indirect (results not shown).

Chromophore molecules were simulated separately, also using the PBE functional. The coefficients c_m and the LUMO energies obtained in these calculations were then used in eq 2.

We underscore that the matrix $\Gamma_{mn}(E)$ calculated using eq 6 or 5 is not dependent on the chromophore, only on its anchoring group, and thus is transferable and can be used for all chromophores with the same anchoring group. The effect of the chromophore on the injection rate $\Gamma_{ss}(E)$ enters eq 2 in the form of the chromophore basis set coefficients c_m and the injection energy E (the chromophore's LUMO energy).

3. RESULTS AND DISCUSSION

3.1. Calculated Injection Times for Dyes on TiO_2. The dye molecules considered in this study are shown in Figure 3. They represent a large set of organic chromophores used in DSSC. In particular, for the six molecules **d**, **h**, and **k**–**n**, experimental

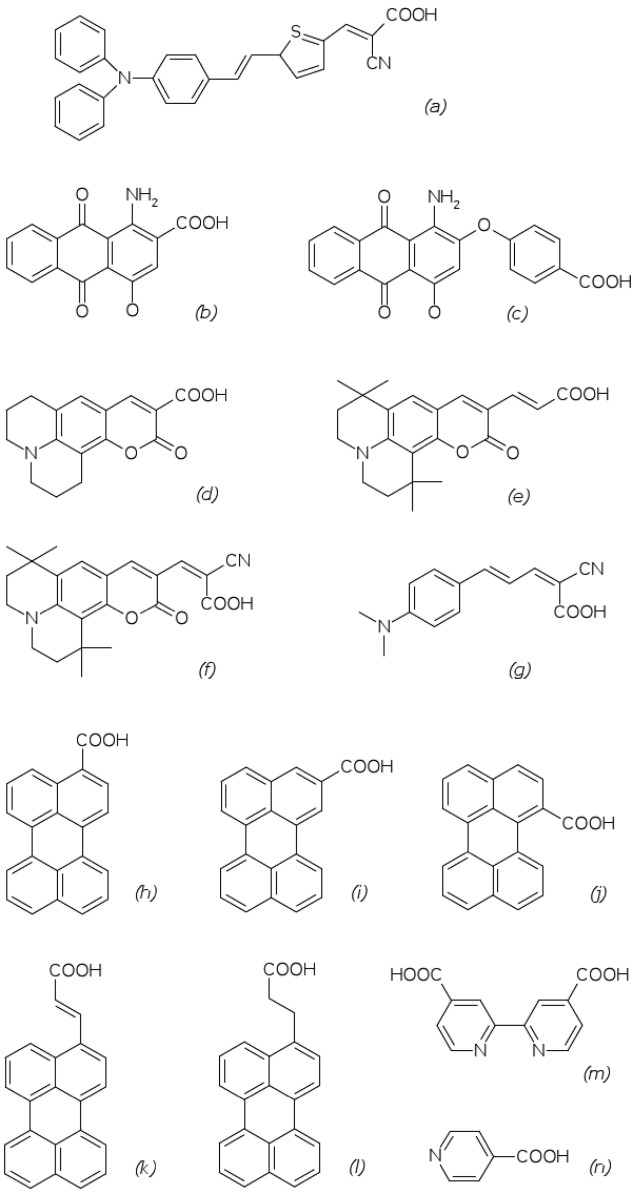

Figure 3. Organic dyes studied in this work.

injection times are available. For molecules **a**−**j**, an alternative theoretical evaluation of the injection time based on simpler cluster calculations is available,[49] as well as experimental DSSC efficiency data.[64−67] Molecules **m** and **n**, biisonicotinic and nicotinic acid, have very fast injection times (less than 3 fs for **m**, measured on the rutile (110) and anatase (101) surface using resonant photoemission spectroscopy[25−27]). Among the perylene derivatives, the COOH (carboxylic acid) and CH═CH−COOH (acrylic acid) derivatives, **h** and **k**, have short injection times, ca. 10 fs,[19−24,68,69] which is faster than that of the propionic acid derivative **l** (injection time 47−57 fs, depending on the TiO_2 polymorph and on experimental conditions[19,22−24,68,69]). Molecule **h** was also predicted to have faster injection times than its isomers **i** and **j** with carboxylic groups in positions 2 and 3.[49] Molecule **d**, coumarin-343 (C343), is one of the early examples of organic dyes for DSSC, the time of its fastest electron injection process has been variously estimated to be between 100 and 200 fs;[11−18] in many of these early experiments the measured injection time was suggested to be the upper limit, restricted by the instrument response.[12,14−16]

For molecules **a**−**g**, we can use the solar power conversion efficiency (PCE) as a rough guide for their efficiency in electron injection. As mentioned in the Introduction, the overall efficiency is affected by rates of all electron transfer processes in a DSSC, and electron injection is rarely the efficiency-determining step. In particular, if electron injection is fast, PCE will be controlled by other processes, such as electron recombination and electron capture by the redox couple, and may not correlate with injection rates; on the other hand, we can expect that poor electron injection systems have significantly reduced PCE. In our set, we have chromophores that produce devices with fairly high values of PCE (dyes **a** and **e**−**g** with PCE of 5.94%,[64] 3.4%,[66] 4.1%[66] and 5.5%,[67] respectively), fairly low PCE (dye **d**, 0.9%[66]), and very low PCE (dyes **b** and **c**: 0.018% and 0.125%, respectively[65]).

The calculated injection times τ_{inj} of chromophores **a**−**n** are presented in Table 1 and are compared with earlier calculations[49] and with experimental values, where available. For each chromophore, we calculated injection times for rutile (110) and anatase (101) slabs of several thicknesses. The mean values of τ_{inj}, averaged over two to four-layer slabs (two to five layers for rutile), are given in Table 1, together with the standard deviations. Injection times for all these dyes and all rutile and anatase slabs considered in this work are given in the Supporting Information, Tables S1−S3.

There is some spread in the calculated τ_{inj} values depending on the number of layers in the slab, but there is no clear dependence on the number of layers. In some cases, especially if injection times are large, the values for the two-layer anatase slab are significantly larger than for the other slabs; the four-layer result is usually the fastest (smallest). For rutile, odd−even oscillations can be seen for approximately half of the molecules, with odd-layer slabs having longer injection times; in some other cases (especially for slow injection), the thinnest slab has the longest injection times. On the basis of our data, it is impossible to say with confidence whether these odd−even oscillations in injection times are a real effect, similar to that observed for surface energies, band gaps, etc. of rutile (110) slabs,[55,56] or are just due to insufficient accuracy of the computational model.

In the following, we use the mean values of injection times averaged over all the slabs considered with different thicknesses. Alternatively, the values for the thickest four-layer anatase slab can be used (these injection times are, in our calculations, on average 12% smaller than the mean values), and for four- or five-layer rutile (these injection times are, on average, 24% and 7% smaller than the mean values reported in Table 1). Thus, the differences between the thickest slab results and the mean values are usually small, and if, for example, the four-layer slab results were to be used instead of the mean values, the nature of the discussion below would not change much.

The injection times for this set of molecules are also plotted in Figure 4, on the logarithmic scale, and ordered according to their injection times (from fastest to slowest) in the rutile (110)−dissociatively adsorbed molecule system. The graph compares our results for molecules **a**−**n** and anatase (101) or rutile (110) surfaces. Our calculated injection times are in qualitative agreement with the earlier predictions[49] (also included in the figure) obtained using TiO_2 clusters, although the values obtained in this work tend to be slightly larger. A significant difference in calculated injection times can be seen only in cases of slow injection.

Table 1. Calculated Injection Times τ_{inj} (with Standard Deviations) for Molecules a−n (See Figure 3), into Anatase (101) and Rutile (110) Slabs, Compared with Earlier Calculations[49] and Experimentally Measured Injection Times

	Injection time, fs						
	on anatase (101)				on rutile (110)		
Molecule	nondissociated (this work)	dissociated (this work)	dissoc. (ref.49)	exp.	dissociated (this work)	dissoc. (ref.49)	exp.
a	97.6 ± 34.8	49.9 ± 16.9	4.3		17.2 ± 4.3	21.1	
b	1314 ± 616	693 ± 482	16.3		33.0 ± 36.5	656	
c	242 ± 73	132 ± 32	73.2		157 ± 163	1584	
d	10.1 ± 1.2	2.8 ± 0.2	1.6	200,[11] 125,[13,17] <100,[14−16] <150[18]	10.0 ± 5.5	1.4	
e	4.8 ± 0.4	4.1 ± 1.2	2.6		11.6 ± 5.0	1.5	
f	26.4 ± 10.4	6.0 ± 2.1	4.1		4.8 ± 3.6	2.2	
g	8.7 ± 1.5	3.7 ± 0.4	2.9		5.6 ± 2.1	0.82	
h	10.8 ± 1.8	2.1 ± 0.7	2.7	13[19,20,68]	3.6 ± 2.1	5.3	9[21,23,68,69]
i	62.0 ± 10.8	5.8 ± 0.5	5.3		21.9 ± 9.5	21.2	
j	10.5 ± 2.6	1.5 ± 0.4	1.9		3.6 ± 1.8	5.1	
k	6.6 ± 0.6	3.4 ± 1.0		10,[19,68] <30[24]	6.0 ± 2.3		13.5[22,69]
l	1601 ± 147	507 ± 53		57,[19,68] 52[24]	1522 ± 691		47[22,2369,]
m	4.1 ± 0.6	1.5 ± 0.5		<7[27]	0.73 ± 0.25		<3[25,26]
n	2.7 ± 0.4	0.64 ± 0.18			0.68 ± 0.41		<5[26]

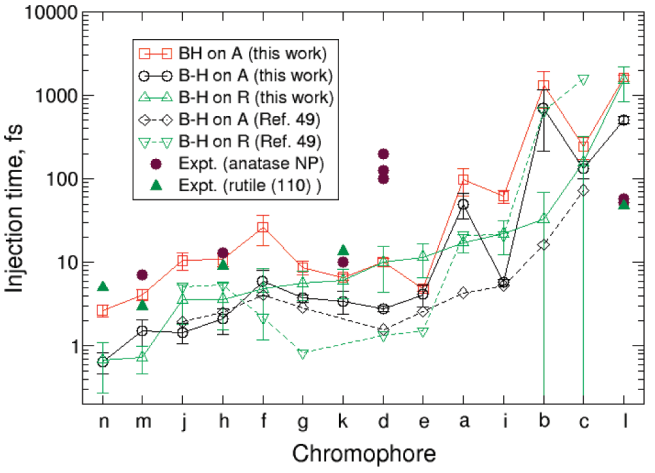

Figure 4. Injection times for dyes shown in Figure 3 and rutile (110) (dissociative adsorption, labeled "B-H on R") or anatase (101) surfaces (dissociative adsorption, labeled "B-H on A", and nondissociative adsorption, labeled "BH on A"), calculated in this work and in ref 49. Molecules **a**−**n** are ordered according to the calculated rates of injection for the "B-H on R" system, from fastest to slowest injection.

Figure 4 also shows that the magnitudes of injection times and their fast-to-slow ordering are broadly similar on anatase (101) and rutile (110) surfaces. This suggests, first, that neither of these TiO_2 polymorphs offers significantly faster electron injection than the other, and any difference in real solar cells can be ascribed to different porosity, morphology, and electron transport within TiO_2 (generally, the semiconductor material used in DSSC is nanoporous TiO_2, consisting mostly of small (∼10 nm) anatase nanoparticles[2,25]). Second, it is likely that injection rates for these chromophores on other TiO_2 surfaces, such as the rutile (101), (111), and (001) surfaces, shown to have a high photocatalytic activity,[70] and anatase (100), (001), and (103) surfaces that occur in anatase nanoparticles,[2,71] should be similar to the ones that we find for the most stable and most commonly found rutile (110) and anatase (101) surfaces. Note that, in an experimental study[72] of chromophores on rutile (110) and (100) surfaces, the value of incident photon-to-current conversion efficiency (IPCE) was much larger for the (100) surface than for (110), but the absorbed photon-to-current conversion efficiency (APCE) was almost the same for both surfaces. The difference in IPCE was attributed to a higher density of adsorbed dyes on the rutile (100) surface than on (110), in support of the idea that injection rates are not strongly dependent on the type of the surface.

One more observation that can be made from the results in Figure 4 and Table 1 is that injection is faster for the dissociatively adsorbed geometry on anatase (101) than for the nondissociative adsorption, despite the larger adsorption energy for the nondissociated geometry. This is not surprising, as the nondissociative adsorption geometry involves only one surface-molecule covalent Ti−O bond and a weaker O···H hydrogen bond, whereas the dissociatively adsorbed geometry has two covalent surface−molecule bonds, i.e., stronger binding and a better channel for the molecule−surface electron transfer than just a single covalent bond and a hydrogen bond.

3.2. Comparison with Experimental PCE and Injection Times. *3.2.1. Comparison with Experimental PCE Values.* PCE is estimated and reported very often for various DSSC implementations; however, as we pointed out in the previous section, PCE is not a direct measure of electron transfer rates, but rather it reflects the combined efficiency of all electron-transfer processes in a DSSC. Some of the loss processes are chromophore-independent (e.g., electron recombination with the electrolyte), and some other elementary steps (such as the chromophore neutralization by the electrolyte) are likely to have similar rates for chromophores of similar chemical nature and energetics as we have here. Nevertheless, we expect that very low values of PCE will correlate with long injection times, whereas medium and high PCE values can be obtained if electron injection is efficient.

We consider a set of dyes, **a**−**g**, and experimental values of PCE for DSSCs based on these dyes. As porous TiO_2 nanoparticles typically used in DSSCs predominantly consist of the anatase polymorphs, the calculated results for anatase slabs are more relevant than those for rutile.

Molecules **b** and **c** form poor DSSC devices with very low PCE.[65] In good agreement with this, our calculated injection times for these dyes are of the order of picoseconds or hundreds of femtoseconds, i.e., electron injection will compete with recombination, possibly leading to a loss of the photoexcited electrons.

Devices based on dyes **a** and **d**−**g** have PCE values between 1% and 6%[64,66,67] (midrange efficiency, lower than the highest PCE of up to 12% obtained with the best ruthenium dyes). Our calculated injection times for these dyes are on the order of femtoseconds or tens of femtoseconds. While there is no one-to-one correspondence between our calculated injection times and experimental PCE values, we can conclude that injection times on the order of tens of femtoseconds are fast enough to ensure that electron injection is significantly faster than competing loss processes and does not limit the efficiency of DSSC.

3.2.2. Comparison with Experimental Injection Times. In Table 1 and Figure 4, we compare our theoretical values of injection times from these dyes into TiO_2 anatase (101) and rutile (110) surfaces with the experimental values. Experimental injection times are available for several types of organic chromophores: perylene-based compounds with different spacer groups: molecules **h**, **k**, **l**;[19−24] isonicotinic and biisonicotinic acids: molecules **m** and **n**;[25−27] and a coumarin dye C343: molecule **d**.[11−18]

The calculated injection times for isonicotinic and biisonicotinic acids, **n** and **m**, are very fast (0.7−4.1 fs) and thus agree well with experimental measurements that find the upper limits of τ_{inj} for these molecules to be 5 and 3 fs for **n** and **m**, respectively, on rutile (110) single crystals,[25,26] and less than 7 fs for **m** on anatase nanoparticles.[27] Our calculations of biisonicotinic acid do not take into account that this molecule has two carboxylic groups, both of which will be bonded to TiO_2[25] and will provide two pathways for electron injection, leading to faster injection than for isonicotinic acid, as shown in experiments.[26] We also note that, as the experimental values are the upper limits (limited by the resolution of the experiments[25−27]), the exact injection times may be even faster than the reported 3−7 fs and may agree even better with our results.

Among the perylene derivatives **h**, **k**, and **l**, the calculated injection times for the molecules with the anchoring carboxylic group connected either directly to the perylene core, as in molecule **h**, or via an unsaturated spacer group, as in molecule **k**, also agree very well with the experimentally measured injection times reported in refs 19−23: 2−11 fs (calculated) against 9−13.5 fs (measured) for both molecules **h** and **k**; very similar values were found for these molecules on rutile (110) single crystals and anatase nanoparticles (or anatase (101) slabs, in the calculations). Our calculated values also agree with the earlier theoretical values of 9.0−16.2 fs[47] and 3−6 fs.[19,48,32,33]

The situation is different for perylene with a saturated spacer group (propionic acid), molecule **l**. Our calculated injection times are of the order of hundreds of femtoseconds or picoseconds, much slower than the experimental values that range between 47 and 57 fs,[22−24] and earlier theoretical predictions of 132 fs[33] and 33 fs[32] obtained using a simple model based on the width of PDOS peaks. The reason for the slow injection predicted by our model for molecule **l** is that the proportion of the LUMO localized on the carboxylic group is very low: the saturated spacer effectively isolates the carboxylic group from the perylene core, where most of the LUMO is located. While both experimental and theoretical results agree that saturated spacer groups decrease the electron injection rate, the decrease predicted by our model is unacceptably low. This is likely due to a change in mechanism of electron tunnelling when a saturated spacer is introduced. We have assumed a direct coupling between the chromophore orbital and the semiconductor, which is reasonable in all cases where the carboxylic group is directly connected to the conjugated moiety. In the case of a saturated bridge, the coupling between chromophore and semiconductor may occur though superexchange:[73] the chromophore orbital is coupled to the bridge (i.e., the spacer group) orbitals, which are in turn coupled to the semiconductor. The corrections required to include superexchange coupling[73] will not be introduced in this paper.

Another molecule with poor agreement between calculated and experimental injection times is C343, molecule **d**. Reported experimental τ_{inj} times for the fastest electron injection process vary between <100 fs[14−16] and ∼200 fs,[11] whereas our calculated values are between 3 and 10 fs. We note that earlier theoretical studies of electron injection using a representation of Hamiltonian in a basis of localized donor and acceptor states[45,46] found fast injection times of 13−20 fs for this molecule, in agreement with our results, but in disagreement with experiment. One of the proposed explanations was that vibrational time scales are relatively close to electron transfer time scales for this molecule, and complete separation between electron transfer dynamics and nuclear motion is not fulfilled;[45] another possible explanation[46] is that combined fast and slow injection processes may effectively result in observed slow injection times. We note that, unlike the relatively recent experiments on biisonicotinic acid and perylene derivatives[19−27] conducted using photoemission spectroscopy in a vacuum, the studies of C343 were mostly done using transient absorption in ambient conditions[13−16] and involve large standard deviations in measured injection times (up to ±50 fs[11]); there is also a large spread of measured τ_{inj} values for C343 (see Table 1). Some of these experimental studies pointed to the resolution limits of their experiments and suggested that the fastest injection time in this system is less than their resolution of ∼100 fs.[14−16] The combination of these arguments suggests that the experimental injection times are not reliable or refer to electron injection processes that are not the fastest for this molecule, and thus should not be used as benchmarks.

In summary, our theoretical model provides a good agreement with experiments in cases of fast injection, although it may fail if injection is very slow, as in this case alternative mechanisms (supexchange, coupling with vibrational modes) may become important.

3.3. Effect of the Anchoring Group's Size on the Calculated Injection Times. To confirm that benzoic acid, the anchoring group used in our electronic-structure calculations, is big enough to reliably represent the coupling between the dye and the TiO_2 surface, we did two additional types of calculations: (i) using formic acid (the smallest carboxylic acid) as an anchoring group, and (ii) using complete chromophores **h** and **l** adsorbed on TiO_2 slabs (the examples of good and poor agreement of the calculated and experimental injection times). Example structures used for calculations (i) and (ii) are shown in Figure 2e,d.

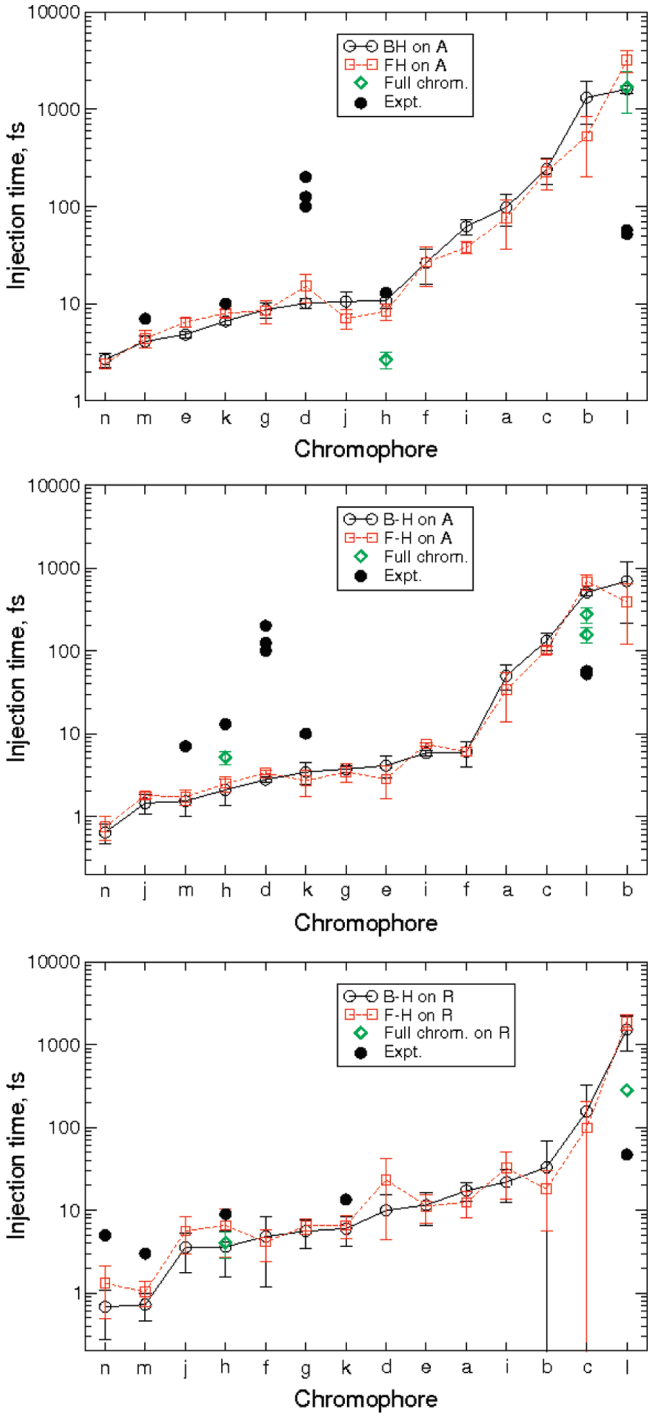

Figure 5. Injection times for dyes shown in Figure 3, calculated using benzoic acid (BH) and formic acid (FH) as anchoring groups on anatase (A) and rutile (R) surfaces. Top panel: calculated using nondissociatively adsorbed anchoring group on anatase (101); middle panel: using dissociatively adsorbed anchoring group on anatase (101); bottom panel: using dissociatively adsorbed anchoring group on rutile (110).

The injection times for dyes **a**−**n** calculated using benzoic acid and formic acid as anchoring groups are compared in Figure 5. We can see that the anchoring group as small as formic acid gives the values of injection times very close to those calculated using the benzoic acid anchoring group. For the molecules on anatase, although the formic acid-based results differ from the benzoic acid-based results by a factor of 2 in a couple of cases, the average difference between the injection times calculated using the two anchoring groups is less than 2%. For rutile, the deviations are somewhat bigger and, on average, injection times calculated using formic acid are 33% greater (mainly due to the large differences found for few molecules: **d**, **h**, and **n**). This shows that even a very small anchoring group, such as formic acid, provides reliable electronic coupling data for calculations of electron transfer times, and the results are very close to those obtained using the larger anchoring group.

Table 2. Electron Injection Times for Dyes h and l, Calculated Using the Benzoic Acid (BA) Anchoring Group or the Complete Chromophore (CC)

	injection time, fs					
	on anatase (101)				on rutile (110)	
	nondissociated		dissociated			
molecule	BA	CC	BA	CC	BA	CC
h	10.8	2.7	2.1	5.2	3.6	4.1
l	1601	1683	507	157, 275[a]	1522	282[b]

[a] Values for two different cell sizes. [b] Calculated only for a two-layer cell.

Figure 5 and Table 2 also present injection times calculated using complete chromophores **h** and **l**, compared to the results obtained using the benzoic acid anchoring group. For the perylene molecule **h**, the injection times obtained in the full-chromophore calculations (2.7−5.2 fs) are very close to those calculated using benzoic acid as an anchoring group (2−11 fs); both are in good agreement with experiment (8.4−13 fs[19−21,23,68,69]).

For perylene **l** with the propionic acid functional group, the injection times in the full-chromophore calculations are on the order of picoseconds or hundreds of femtoseconds, depending on the adsorption mode and on the cell geometry, and are smaller but similar to those obtained using the benzoic acid anchoring group. Thus, the disagreement with experiment is not due to the insufficiently accurate description of the dye-TiO_2 interface using the small anchoring group model.

On the basis of this comparison, we can conclude that our approach of separating the complete TiO_2−choromophore system into fragments provides an accurate description of the electronic structure of the full system and a good estimate of electron injection times. By separating the system into fragments, we can obtain injection times that compare well with those calculated using the full system, but in a significantly lower computational time.

3.4. Accuracy and Effect of the LUMO Energy Values. In our calculations, we used the LUMO energy of the neutral molecule in its ground state as the energy of electron injection into the conduction band of TiO_2, neglecting electron exchange and charging effects. The LUMO is generally not the same as the highest (singly) occupied orbital of a molecule in its excited state (the state from which electron injection in DSSC takes place). Moreover, DFT is a ground-state theory, and the virtual orbitals in DFT do not have a rigorous physical meaning. In particular, GGA functionals (such as the PBE functional used in this work) are known to underestimate band gaps. This concerns both the molecules' HOMO−LUMO gaps and the band gap of TiO_2. The energies of excited states can be evaluated more accurately using

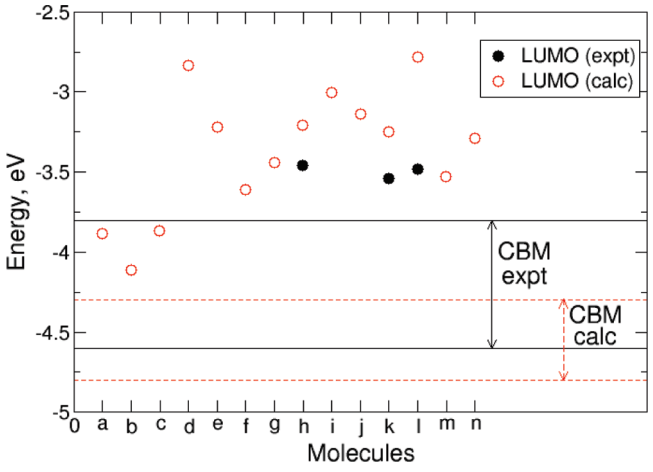

Figure 6. Calculated and experimental[69] chromophores' LUMO energies (open and filled circles, respectively), compared with the range of calculated TiO_2 CBM values for rutile (110) and anatase (101) slabs of different thicknesses with adsorbed benzoic acid (the highest and lowest calculated CBM values are shown by dashed lines) and the range of experimental TiO_2 CBM for rutile samples with and without adsorbates (from workfunction measured by two-photon photoemission[69]), solid lines.

the state-of-the-art TD-DFT method;[74] also, new long-range corrected DFT functionals have been developed,[75−77] which are able to describe charge-separated states; these are, however, not used here. The implicit assumption in the DFT studies of virtual orbitals' alignment is that the molecules' LUMO energies and the conduction band minimum (CBM) of the semiconductor are underestimated by approximately the same amount, and the error in the evaluation of these energies may cancel. The relative positions and the alignment of the energy levels of chromophores and TiO_2 is crucial in electron transfer processes in DSSC, because the electron injection process relies on the presence of TiO_2 states, at the same energy as the chromophore's LUMO, available to accept an electron. There is inherent inaccuracy in our calculations of the dyes' LUMO energies and their alignment with the TiO_2 conduction band, due to the limitations of the DFT-GGA method used here. Therefore, it is essential to evaluate the error in the calculated chromophores' LUMO energies and TiO_2 conduction band energies and to make an estimate of how this will affect calculated injection times.

The position of the CBM of TiO_2 measured using photoemission spectroscopy is 3.8−4.6 eV below the vacuum level.[22,69] In our calculations, the CBM varies between −4.4 and −4.8 eV for rutile (110), and between −4.3 and −4.6 eV for anatase (101) slabs with adsorbates, in reasonable agreement with experiments. Thus, there is no need to apply a shift to the calculated conduction band energies. (We note that, on the contrary, the calculated valence band maximum (VBM), −6.1 to −6.6 eV, is ∼1.5 eV higher than its experimental position, 7.5−8.0 eV below the vacuum level.[22,69] By comparison, our recent calculations[55] of TiO_2 slabs without adsorbate using the B3LYP hybrid functional[78] gave the VBM position close to the experimental values, but the CBM was ∼0.5 eV too high).

We also compare the calculated HOMO and LUMO energies of (gas-phase) perylene derivatives **h**, **k**, **l** with the experimentally measured values for these molecules adsorbed on TiO_2 rutile[69] (Figure 6). Like in the case of TiO_2, the calculated HOMOs are ∼1.5 eV too high (not shown); but the calculated LUMOs are

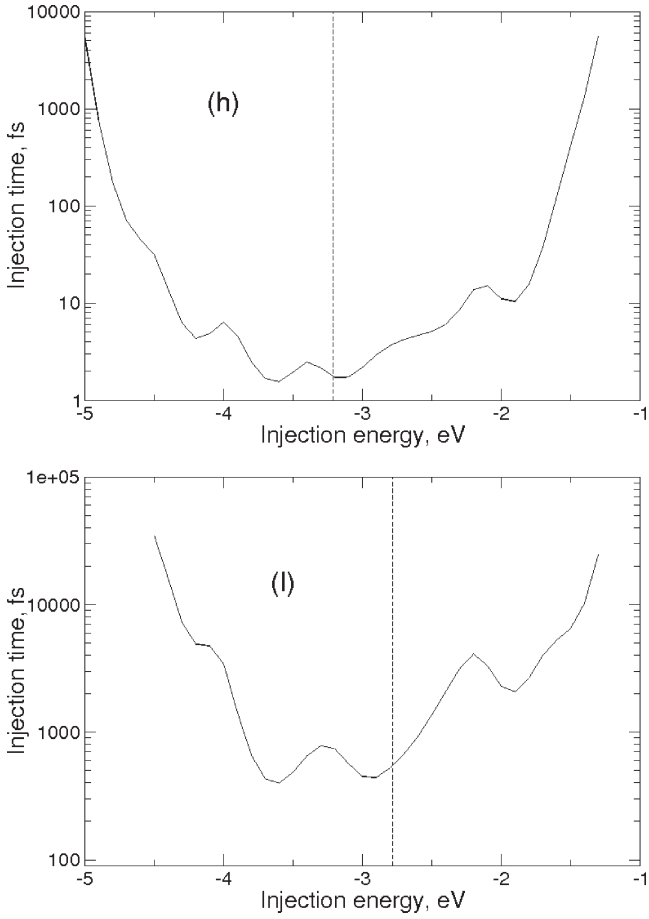

Figure 7. Injection times for chromophores **h** and **l** on a four-layer rutile (110) slab for a range of injection energies *E*. The vertical dashed lines show the positions of the chromophores' LUMOs.

quite close to their experimentally measured positions (usually within 0.5 eV). Note that the experiments in ref 69 deal with the perylene derivatives adsorbed on TiO_2, and the energy levels of adsorbed molecules may be somewhat shifted compared to isolated molecules; thus, the agreement with our calculations may be fortuitous. We are not aware of experimental measurements of electron affinities or LUMO energies of these molecules in the gas phase, to compare with our calculations.

We cannot be certain that the error in the calculated LUMO energies is systematic for all types of chromophores (indeed, we find that for polyaromatic hydrocarbons the LUMO energies tend to be too low by ∼2.0 eV (results not shown)). However, the calculated TiO_2 CBM energies and perylene derivatives' LUMO energies are in fairly good agreement with experiment. Therefore, throughout this paper, we have used our calculated energies of these states, both for TiO_2 and for all chromophores, without applying any corrections to adjust them.

To check the effect of the possible inaccuracy in alignment of the dyes' LUMO levels with the TiO_2 conduction band, we calculated injection times for molecules **h** and **l** on rutile (110) using a range of injection energies *E* (but always using the dyes' LUMO wave function coefficients; see Figure 7). The injection times for chromophore **h** are smaller than 10 fs in a wide interval of injection energies, from the bottom of the conduction band to −2 eV, and are rather weakly dependent on the energy in this interval. Similarly, for dye **l**, injection times are of the order of

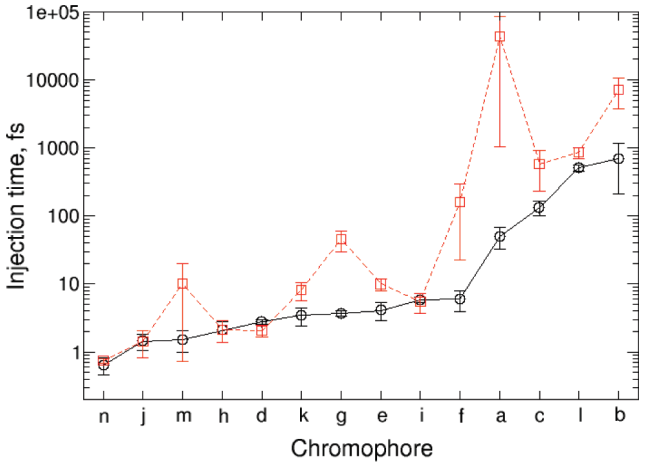

Figure 8. Electron injection times for chromophores **a**−**n** on rutile (110), calculated using the chromophores' LUMO energies as injection energies (black circles) and using injection energies shifted by −0.5 eV (red squares).

hundreds of femtoseconds in the interval of injection energies equivalent to the lower half of the TiO_2 conduction band, i.e., the overestimation of the injection time is not due to the incorrect position of the LUMO. As a further test, we calculated injection times for dyes **a**−**n**, using the injection energies 0.5 eV lower than the respective calculated LUMO energies. Figure 8 shows that, for all these chromophores, changes in injection times due to this shift in the LUMO energies are fairly small: although the exact fast-to-slow ordering changes, the molecules with fast injection times remain fast, and slow injection is also not significantly changed. The sensitivity of injection times to chosen injection energies is larger for those molecules (**m**, **g**, **f**, **a**, **c**, and **b**), whose LUMO energies are close to the conduction band edge, where the TiO_2 density of states varies more strongly with energy. Therefore, if the calculated LUMO energies are incorrect by ±0.5 eV, it most likely will not lead to a qualitative difference in calculated injection times.

4. DISCUSSION AND CONCLUSIONS

The aim of this paper was to predict electron injection times from dye molecules into TiO_2, using the approach of partitioning the TiO_2−dye system into fragments (TiO_2 slab with adsorbed anchoring group, and an isolated dye) and calculating the imaginary part of the self-energy $\Gamma_{ss}(E)$ (the lifetime of the excited state of the dye adsorbed on TiO_2) using the electronic properties of the fragments: density of states of TiO_2, TiO_2−anchoring group coupling, and dyes' LUMO wave function coefficients. Using the partitioning approach, the description of the TiO_2−anchoring group interface can be done once and reused for all molecules with the same anchoring group (carboxylic acid in this study), and only a calculation of the isolated dye's electronic structure and LUMO orbital is required for each dye.

We investigate a large set of molecules and compare our calculated electron injection times with experimental results. We show that injection times calculated using this approach are, with few explainable exceptions, in good agreement with experimental results on dyes' injection times and on efficiencies of solar cells based on these dyes.

Our results demonstrate that separation of the TiO_2−dye system into fragments and considering an anchoring group, rather than a full chromophore, in density of states and electronic coupling calculations, is a valid approximation, which leads to good qualitative and quantitative agreement between injection times calculated both using fragments and using the full system, and experimental injection times. The benefit of separating the system into fragments is the much shorter computational time of electronic structure calculations, both because of the smaller number of atoms in the anchor molecule, the smaller TiO_2 slab needed to ensure sufficient separation between adsorbed molecules, and because we do not need to determine the exact adsorption geometry of the large chromophore molecules.

Thus, whereas most theoretical studies consider adsorption of full chromophores and, consequently, have to focus on one or few molecules, our model allows us to do a systematic study of many chromophores. Such high-throughput studies of large numbers of chromophores can be useful for experimental groups designing dyes for DSSCs, as electron injection properties of candidate dyes can be evaluated before the dyes are synthesized.

There are several open questions in the theoretical description of electron transfer processes. One of them is the accuracy of evaluation of the injection energy (represented either as the LUMO energy or, more accurately, as the excited state energy). The LUMO energies and, possibly, even the LUMO−conduction band alignment are likely to be dependent on the computational approach, e.g., on the choice of the exchange-correlation functional in DFT calculations. In general, DFT does not give an accurate description of the molecule's excites states; a more reliable description can be provided by TD-DFT, together with long-range corrected DFT functionals.

Accurate computational chemistry studies on few selected test systems can give us information about the accuracy and suitability of different exchange-correlation functionals for evaluation of electronic energies. A study like this one, dedicated to screening of a large set of chromophores and evaluation of the chromophores' injection times, can be quickly repeated if new density functionals with much improved performance for TiO_2 become available. On the other hand, this study is not suitable for validation of different density functionals: validation of functionals should be performed using experimental properties more directly related to the computations (e.g., optical band gap, electron affinity, ionization potential), rather than properties such as injection time, which depend on many parameters so that the effect of the functional would be difficult to single out.

Another issue is the shift of the TiO_2 conduction band due to coadsorbents present in the electrolyte (for example, Li^+ ions, 4-*tert*-butylpyridine or chenodioxycholic acid),[79,80] and due to the nature of the solvent environment itself.[81] This shift will necessarily change the position of the dye's LUMO relative to the conduction band, and therefore affect injection times. As a result, injection times can change[79] by up to several orders of magnitude.[81] We did not address this in the paper, but we provide an error bar for injection times due to an uncertainty in the relative positions of the dye's LUMO and the TiO_2 conduction band. According to our results in Figure 8, the sensitivity of injection times to TiO_2 CBM position is larger if the injection energy is close to the conduction band edge.

One more factor that can affect injection efficiency is the decay lifetime of the dye's excited state. The injection efficiency can be evaluated as $\eta_{inj} = k_{inj}/(k_{inj} + k_0)$, where k_{inj} is the injection rate (the inverse of the injection time τ_{inj}), and k_0 is the inverse of the excited state decay lifetime.[82] If excited state decay is fast, then this additional decay pathway competes with injection in TiO_2,

and the injection efficiency can be significantly reduced.[82,83] The decay time is one of the most elusive quantities in quantum chemistry[84] (for example, it is still not possible to predict whether a molecule will fluoresce), and we do not address it in this paper.

Despite the approximations used in this study, the agreement of our calculated injection times with experimental injection times and DSSC efficiencies is qualitatively very good, and we can be certain that molecules with predicted fast injection times (femtoseconds and tens of femtoseconds) do indeed provide good electron injection. To apply our method further, we are planning to model injection time for dyes with other anchoring groups, e.g., phosphonic acid, and for organometallic porphyrine dyes, to investigate the effect of the dyes' anchoring groups and aromatic or porphyrine cores.

■ ASSOCIATED CONTENT

Supporting Information. A table of injection times for dyes **a**−**m** and all TiO_2 slabs considered: 2, 3, 4, and 5-rutile (110) and two, three, and four-layer anatase (101) slabs. This material is available free of charge via the Internet at http://pubs.acs.org.

■ AUTHOR INFORMATION

Corresponding Author

*E-mail: N.Martsinovich@warwick.ac.uk; A.Troisi@warwick.ac.uk.

■ ACKNOWLEDGMENT

We acknowledge financial support from the European Research Council (ERC).

■ REFERENCES

(1) O'Reagan, B.; Grätzel, M. *Nature* **1991**, *353*, 737.
(2) Grätzel, M. *J. Photochem. Photobiol. C* **2003**, *4*, 145–153.
(3) Moreira Gonçalves, L.; de Zea Bermudez, V.; Aguilar Ribeiro, H.; Magalhães Mendes, A. *Energy Environ. Sci.* **2008**, *6*, 655–667.
(4) Preat, J.; Jacquemin, D.; Perpète, E. A. *Energy Environ. Sci.* **2010**, *7*, 891–904.
(5) Chiba, Y.; Islam, A.; Watanabe, Y.; Komiya, R.; Koide, N.; Han, L. Y. *Jpn. J. Appl. Phys.* **2006**, *45*, L638–L640.
(6) Kroon, J. M.; Bakker, N. J.; Smit, H. J. P.; Liska, P.; Thampi, K. R.; Wang, P.; Zakeeruddin, S. M.; Grätzel, M.; Hinsch, A.; Hore, S.; Wurfel, U.; Sastrawan, R.; Durrant, J. R.; Palomares, E.; Pettersson, H.; Gruszecki, T.; Walter, J.; Skupien, K.; Tulloch, G. E. *Prog. Photovoltaics Res. Appl.* **2007**, *15*, 1–18.
(7) Durrant, J. R.; Haque, S. A.; Palomares, E. *Coord. Chem. Rev.* **2004**, *248*, 1247–1257.
(8) Prezhdo, O. V.; Duncan, W. R.; Prezhdo, V. V. *Acc. Chem. Res.* **2008**, *41*, 339–348.
(9) Asbury, J. B.; Ellingson, R. J.; Ghosh, H. N.; Ferrere, S.; Nozik, A. J.; Lian, T. *J. Phys. Chem. B* **1999**, *103*, 3110–3119.
(10) Asbury, J. B.; Hao, E.; Wang, Y.; Lian, T. *J. Phys. Chem. B* **2000**, *104*, 11957.
(11) Rehm, J. M.; McLendon, G. L.; Nagasawa, Y.; Yoshihara, K.; Moser, J.; Grätzel, M. *J. Phys. Chem.* **1996**, *100*, 9577–9578.
(12) Murakoshi, K.; Yanagida, S.; Capel, M.; Castner, E. W. *Nanostruct. Mater. — Clusters, Compos. Thin Films* **1997**, *679*, 221–238.
(13) Ghosh, H. N.; Asbury, J. B.; Lian, T. *J. Phys. Chem. B* **1998**, *102*, 6482–6486.
(14) Wachveitl, J.; Huber, R.; Spörlein, S.; Moser, J. E.; Grätzel, M. *Int. J. Photoenergy* **1999**, *1*, 1–3.
(15) Huber, R.; Moser, J. E.; Grätzel, M.; Wachveitl, J. *Chem. Phys.* **2002**, *285*, 39–45.
(16) Hao, E. C.; Anderson, N. A.; Asbury, J. B.; Lian, T. *J. Phys. Chem. B* **2002**, *106*, 10191–10198.
(17) Frontiera, R. R.; Dasgupta, J.; Mathies, R. A. *J. Am. Chem. Soc.* **2009**, *131*, 15630–15633.
(18) Stockwell, D.; Yang, Y.; Huang, J.; Anfuso, C.; Huang, Z. Q.; Lian, T. *J. Phys. Chem. C* **2010**, *114*, 6560–6566.
(19) Wang, L.; Ernstorfer, R.; Willig, F.; May, V. *J. Phys. Chem. B* **2005**, *109*, 9589–9595.
(20) Ernstorfer, R.; Gundlach, L.; Felber, S.; Storck, W.; Eichberger, R.; Willig, F. *J. Phys. Chem. B* **2006**, *110*, 25383–25391.
(21) Gundlach, L.; Ernstorfer, R.; Willig, F. *J. Phys. Chem. C* **2007**, *111*, 13587–13594.
(22) Gundlach, L.; Ernstorfer, R.; Willig, F. *Prog. Surf. Sci.* **2007**, *82*, 355–377.
(23) Gundlach, L.; Letzig, T.; Willig, F. *J. Chem. Sci.* **2009**, *121*, 561–574.
(24) Bartelt, A. F.; Schutz, R.; Neubauer, A.; Harmappel, T.; Eichberger, R. *J. Phys. Chem. C* **2009**, *113*, 21233–21241.
(25) Schnadt, J.; Brühwiler, P. A.; Patthey, L.; O'Shea, J. N.; Södergren, S.; Odelius, M.; Ahuja, R.; Karis, O.; Bässler, M.; Persson, P.; Siegbahn, H.; Lunell, S.; Mårtensson, N. *Nature* **2002**, *418*, 620–623.
(26) Schnadt, J.; O'Shea, J. N.; Patthey, L.; Kjeldgaard, L.; Ahlund, J.; Nilson, K.; Schiessling, J.; Krempasky, J.; Shi, M.; Karis, O.; Glover, C.; Siegbahn, H.; Mårtensson, N.; Brühwiler, P. A. *J. Chem. Phys.* **2003**, *119*, 12462–12472.
(27) Schnadt, J.; Henningsson, A.; Andersson, M. P.; Karlsson, P. G.; Uvdal, P.; Siegbahn, H.; Brühwiler, P. A.; Sandell, A. *J. Phys. Chem. B* **2004**, *108*, 3114–3122.
(28) Ghosh, H. N. *J. Phys. Chem. B* **1999**, *103*, 10382–10387.
(29) Persson, P.; Lunell, S.; Ojamäe, L. *Chem. Phys. Lett.* **2002**, *364*, 469–474.
(30) Nilsing, M.; Persson, P.; Ojamäe, L. *Chem. Phys. Lett.* **2005**, *415*, 375–380.
(31) Lundqvist, M. J.; Nilsing, M.; Persson, P.; Ojamäe, L. *Int. J. Quantum Chem.* **2006**, *106*, 3214–3234.
(32) Persson, P.; Lundqvist, M. J.; Ernstorfer, R.; Goddard, W. A., III; Willig, F. *J. Chem. Theor. Comput.* **2006**, *2*, 441–451.
(33) Nilsing, M.; Persson, P.; Lunell, S.; Ojamäe, L. *J. Chem. Phys.* **2007**, *111*, 12116–12123.
(34) Labat, F.; Ciofini, I.; Hratchian, H. P.; Frisch, M.; Raghavachari, K.; Adamo, C. *J. Am. Chem. Soc.* **2009**, *131*, 14290–14298.
(35) Anderson, P. W. *Phys. Rev.* **1961**, *124*, 41.
(36) Muscat, J. P.; Newns, D. M. *Prog. Surf. Sci.* **1978**, *9*, 1.
(37) Stier, W.; Prezhdo, O. V. *J. Phys. Chem. B* **2002**, *106*, 8047–8054.
(38) Duncan, W. R.; Stier, W. M.; Prezhdo, O. V. *J. Am. Chem. Soc.* **2005**, *127*, 7941–7951.
(39) Duncan, W. R.; Prezhdo, O. V. *J. Am. Chem. Soc.* **2008**, *130*, 9756.
(40) Fischer, S. A.; Duncan, W. R.; Prezhdo, O. V. *J. Am. Chem. Soc.* **2009**, *131*, 15483.
(41) De Angelis, F.; Fantacci, S.; Selloni, A.; Nazeeruddin, M. K.; Grätzel, M. *J. Am. Chem. Soc.* **2007**, *129*, 14156.
(42) Venkataraman, C.; Soudackov, C. V.; Hammes-Schiffer, S. *J. Phys. Chem. C* **2010**, *114*, 487–496.
(43) Rego, L. G. C.; Batista, V. S. *J. Am. Chem. Soc.* **2003**, *125*, 7989.
(44) Abuabara, S. G.; Rego, L. G. C.; Batista, V. S. *J. Am. Chem. Soc.* **2005**, *127*, 18234–18242.
(45) Kondov, I.; Thoss, M.; Wang, H. *J. Phys. Chem. A* **2006**, *110*, 1364–1374.
(46) Kondov, I.; Čížek, M.; Benesch, C.; Wang, H.; Thoss, M. *J. Phys. Chem. C* **2007**, *111*, 11970–11981.
(47) Li, J. R.; Nilsing, M.; Kondov, I.; Wang, H. B.; Persson, P.; Lunell, S.; Thoss, M. *J. Phys. Chem. C* **2008**, *112*, 12326–12333.
(48) Wang, L.; Willig, F.; May, V. *Mol. Simul.* **2006**, *32*, 765–781.
(49) Jones, D. R.; Troisi, A. *Phys. Chem. Chem. Phys.* **2010**, *12*, 4625.

(50) Mukamel, S. *Principles of Nonlinear Optical Spectroscopy*; Oxford University Press: New York, 1995.
(51) Nitzan, A. *Chemical Dynamics in Condensed Phases: Relaxation, Transfer and Reactions in Condensed Molecular Systems*; Oxford University Press: Oxford/New York, 2006.
(52) Löwdin, P.-O. *J. Chem. Phys.* **1950**, *18*, 365.
(53) Vittadini, A.; Rotzinger, F. P.; Selloni, A.; Grätzel, M. *J. Phys. Chem. B* **2000**, *104*, 1300–1306.
(54) Li, S.-C.; Wang, J.-G.; Jacobson, P.; Gong, X.-Q.; Selloni, A.; Diebold, U. *J. Am. Chem. Soc.* **2009**, *131*, 980–984.
(55) Martsinovich, N.; Jones, D. R.; Troisi, A. *J. Phys. Chem. C* **2010**, *114*, 22659–22670.
(56) Bates, S. P.; Kresse, G.; Gillan, M. J. *Surf. Sci.* **1998**, *409*, 336–349.
(57) Nilsing, M.; Lunell, S.; Persson, P.; Ojamäe, L. *Surf. Sci.* **2005**, *582*, 49–60.
(58) Ojamäe, L.; Aulin, C.; Pedersen, H.; Kall, P.-O. *J. Colloid Interface Sci.* **2006**, *296*, 71–78.
(59) Soler, J. M.; Artacho, E.; Gale, J. D.; García, A.; Junquera, J.; Ordejón, P.; Sánchez-Portal, D. *J. Phys.: Condens. Matter* **2002**, *14*, 2745–2779.
(60) Perdew, J. P.; Burke, K.; Ernzerhof, M. *Phys. Rev. Lett.* **1996**, *77*, 3865–3868.
(61) Bredow, T.; Aprà, E.; Catti, M.; Pacchioni, G. *Surf. Sci.* **1998**, *418*, 150–165.
(62) Bredow, T. *Int. J. Quantum Chem.* **1999**, *75*, 127–132.
(63) Sánchez-de-Armas, R.; Oviedo López, J.; San-Miguel, M. A.; Sanz, J. F.; Ordejón, P.; Pruneda, M. *J. Chem. Theory Comput.* **2010**, *6*, 2856–65.
(64) Hagberg, D. P.; Yum, J. H.; Lee, H.; De Angelis, F.; Marinado, T.; Karlsson, K. M.; Humphry-Baker, R.; Sun, L. C.; Hagfeldt, A.; Grätzel, M.; Nazeeruddin, M. K. *J. Am. Chem. Soc.* **2008**, *130*, 6259–6266.
(65) Li, C. Y.; Yang, X. C.; Chen, R. K.; Pan, J. X.; Tian, H. N.; Zhu, H. J.; Wang, X. N.; Hagfeldt, A.; Sun, L. C. *Sol. Energy Mater. Sol. Cells* **2007**, *91*, 1863–1871.
(66) Hara, K.; Sato, T.; Katoh, R.; Furube, A.; Ohga, Y.; Shinpo, A.; Suga, S.; Sayama, K.; Sugihara, H.; Arakawa, H. *J. Phys. Chem. B* **2003**, *107*, 597–606.
(67) Hara, K.; Kurashige, M.; Ito, S.; Shinpo, A.; Suga, S.; Sayama, K.; Arakawa, H. *Chem. Commun.* **2003**, 252–253.
(68) Ernstorfer, R., Ph.D. Thesis, Freie Universität Berlin, 2004; http://www.diss.fu-berlin.de/2004/268/.
(69) Gundlach, L., Ph.D. Thesis, Freie Universität Berlin, 2005; http://www.diss.fu-berlin.de/2005/269/.
(70) Morris Hotsenpiller, P. A.; Bolt, J. D.; Farneth, W. E.; Lowekamp, J. B.; Rohrer, G. S. *J. Phys. Chem. B* **1998**, *102*, 3216.
(71) Zimmermann, C.; Willig, F.; Ramakrishna, S.; Burfeindt, B.; Pettinger, B.; Eichberger, R.; Storck, W. *J. Phys. Chem. B* **2001**, *105*, 9245–9253.
(72) Imanishi, A.; Suzuki, H.; Onashi, N.; Ohta, T.; Nakato, Y. *Inorg. Chim. Acta* **2008**, *361*, 718.
(73) Ratner, M. A. *J. Phys. Chem.* **1990**, *94*, 4877–4883.
(74) Runge, E.; Gross, E. K. U. *Phys. Rev. Lett.* **1984**, *52*, 997–1000.
(75) Yanai, T.; Tew, D. P.; Handy, N. C. *Chem. Phys. Lett.* **2004**, *393*, 51.
(76) Chiba, M.; Tsuneda, T.; Hirao, K. *J. Chem. Phys.* **2006**, *124*, 144106.
(77) Vydrov, O. A.; Heyd, J.; Krukau, A. V.; Scuseria, G. E. *J. Chem. Phys.* **2006**, *125*, 074106.
(78) Becke, A. D. *J. Chem. Phys.* **1993**, *98*, 5648–5652.
(79) Koops, S. E.; O'Reagan, B. C.; Barnes, P. R. F.; Durrant, J. R. *J. Am. Chem. Soc.* **2009**, *131*, 4808–4818.
(80) Morandeira, A.; López-Duarte, I.; O'Reagan, B.; Martínez-Diaz, M. V.; Forneli, A.; Palomares, E.; Torres, T.; Durrant, J. R. *J. Mater. Chem.* **2009**, *19*, 5016–5026.
(81) Bartelt, A. F.; Schütz, R.; Neubauer, A.; Hannappel, T.; Eichberger, R. *J. Phys. Chem. C* **2009**, *113*, 2133–2141.
(82) Listorti, A.; López-Duarte, I.; Martínez-Diaz, M. V.; Torres, T.; DosSantos, T.; Barnes, P. R. F.; Durrant, J. R. *Energy Environ. Sci.* **2010**, *3*, 1573–1579.
(83) Koops, S. E.; Barnes, P. R. F.; O'Reagan, B. C.; Durrant, J. R. *J. Phys. Chem. C* **2010**, *114*, 8054–8061.
(84) *Computational Photochemistry*; Olivucci, M., Ed.; Elsevier: Amsterdam, 2005.